

Article

CO Oxidation Catalyzed by Au Dispersed on SBA-15 Modified with TiO₂ Films Grown via Atomic Layer Deposition (ALD)

Xiangdong Qin [†], Wang Ke [‡], Yovanny Vazquez, Ilkeun Lee and Francisco Zaera ^{*ID}

Department of Chemistry and UCR Center for Catalysis, University of California, Riverside, CA 92521, USA; qinxdong@gmail.com (X.Q.); kewang8243@foxmail.com (W.K.); yovannyv25@gmail.com (Y.V.); ilkeun@ucr.edu (I.L.)

* Correspondence: zaera@ucr.edu

[†] Present Address: ASM America, Phoenix, AZ 85034, USA.

[‡] Present Address: Xi'an Aeronautics Computing Technique Research Institute, AVIC, Xi'an 710068, China.

Abstract: It has been established that gold, when in nanoparticle (NP) form and in contact with reducible oxides, can promote oxidation reactions under mild conditions. Here, we report results from our exploration of the catalytic oxidation of carbon monoxide using catalysts where Au NPs were combined with thin titanium oxide films deposited on SBA-15 using atomic layer deposition (ALD). Both orders of deposition, with TiO₂ added either before or after Au dispersion, were tested for two titania film thicknesses amounting to about half and full TiO₂ monolayers. The resulting catalysts were characterized using various techniques, mainly electron microscopy and N₂ adsorption-desorption isotherms, and the kinetics of the oxidation of CO with O₂ were followed using infrared absorption spectroscopy. A synergy between the Au and TiO₂ phases as it relates to the bonding and conversion of CO was identified, the tuning of which could be controlled by varying the synthetic parameters. The ALD of TiO₂ films proved to be an effective way to maximize the Au-TiO₂ interface sites, and with that help with the activation of molecular oxygen.

Keywords: CO oxidation; gold catalysis; titanium oxide; atomic layer deposition; infrared absorption spectroscopy; adsorption-desorption isotherms; kinetics; metal-oxide interface catalytic sites; reducible oxide films



Citation: Qin, X.; Ke, W.; Vazquez, Y.; Lee, I.; Zaera, F. CO Oxidation Catalyzed by Au Dispersed on SBA-15 Modified with TiO₂ Films Grown via Atomic Layer Deposition (ALD). *Catalysts* **2023**, *13*, 1106. <https://doi.org/10.3390/catal13071106>

Academic Editors: Hongxing Dai and Junhu Wang

Received: 23 June 2023

Revised: 11 July 2023

Accepted: 14 July 2023

Published: 15 July 2023



Copyright: © 2023 by the authors. Licensee MDPI, Basel, Switzerland. This article is an open access article distributed under the terms and conditions of the Creative Commons Attribution (CC BY) license (<https://creativecommons.org/licenses/by/4.0/>).

1. Introduction

Oxidation reactions are quite prevalent in industrial processes, but their selective promotion is difficult to achieve; the thermodynamically favored products from the oxidation of organic reactants are carbon dioxide and water [1–4]. To avoid full oxidation, this catalysis needs to be carried out under mild conditions. It turns out that an excellent candidate for such processes is gold; although bulk Au is typically inert, it has been shown that in nanoparticle (NP) form Au displays remarkable catalytic behavior [5–10]. In fact, we have shown in the past that Au-TiO₂ yolk-shell catalysts, upon proper pretreatment, are capable of oxidizing carbon monoxide at cryogenic temperatures [11–14]. Two requirements have been identified as being critical in defining the performance of Au-based catalysts: (1) the size of the metal NPs, and (2) the nature of the oxide upon which these NPs are dispersed [15]. Regarding the second point, it is generally believed that the catalytic sites are at the interface between the metal and the underlying oxide, which needs to be easily reducible [15–20]. Therefore, it would be highly desirable to be able to tune such an interface at the molecular level.

We have been exploring a way to do this using atomic layer deposition (ALD), a method that affords tuning of the thickness of the active oxide film in contact with the metal NPs at a sub-monolayer level [21–25]. Here, we report results from our initial studies with catalysts made by combining the deposition of small Au NPs and thin titania films on a well-defined silica support, namely, on mesoporous SBA-15. The thickness of the titania

film was kept below or around one monolayer by restricting the number of ALD cycles used for its deposition in order to also probe the possibility of creating new titania–silica mixed-oxide surface sites [26–30]. The order in which the Au NPs and TiO₂ thin films are deposited on the SBA-15 support was tested, as indicated schematically in Figure 1. We show that, indeed, our catalysts are able to promote the oxidation of CO at low temperatures and using O₂ as the oxidant. Moreover, we report that there is a synergy between the metal and oxide phases that helps to enhance the catalytic activity. The incorporation of ALD as a way to synthesize oxide-based catalysts provides unique catalytic tunability not easy to achieve via more conventional means.

TiO₂ ALD + Au NP Deposition on Porous Materials

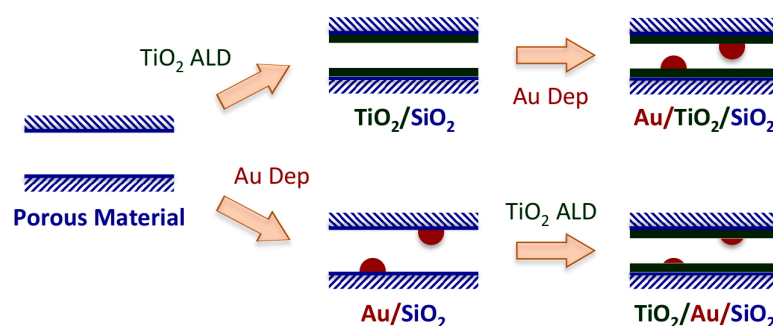


Figure 1. Scheme of the Au + (x ALD-TiO₂) catalyst synthesis strategy used in this work, emphasizing the two options available in terms of the sequence in which the Au nanoparticles and TiO₂ films are added to the SBA-15 (silica) support.

2. Results

The quality of the TiO₂ films deposited via ALD was checked first by acquiring N₂ adsorption–desorption isotherms to obtain pore size distributions. Given the uniform pore size in SBA-15, such pore size distributions can be used to assess the uniformity of the deposited films, as we have shown in the past [26]. Figure 2 summarizes some key results from this characterization. It was determined that the original SBA-15 pores exhibit an average diameter of approximately 6.6 nm, with a size distribution peak with a half-width-at-half-maximum of 0.6 nm. This distribution is not affected in any significant way by the addition of Au NPs directly on the silica surface (Figure 2, left panel: green filled circles and long dashed lines). On the other hand, the deposition of the titania films reduces the size of the pores, as expected [31]. After one TiO₂ ALD cycle, the measured average pore diameters were 6.4 ± 0.3 nm in both samples where Au deposition was carried out before or after the titania ALD (Figure 2, left panel: blue open squares and solid lines; right panel: blue filled squares and short dashed lines, respectively); the corresponding values after two TiO₂ ALD cycles were 5.9 ± 0.3 nm (Figure 2, left panel: red filled diamonds and short dashed lines; right panel: red open diamonds and solid lines, respectively). For comparison, the value obtained after performing two TiO₂ ALD cycles directly on SBA-15, without any addition of Au, was 5.9 ± 0.3 nm as well (Figure 2, right panel: purple open circles and long–short dashed lines). In previous studies, we determined that, after an initial larger pore size decrease in the first TiO₂ ALD cycle, steady film growth takes place at a linear rate of 1.15 ± 0.15 Å/cycle [31]; this behavior was reproduced here. For the purposes of this study, two main conclusions can be derived from the new data: (1) the TiO₂ films are quite uniform, as the pore size distribution retains its narrow nature after the ALD processes (the half-width-at-half-maximum is approximately the same in all cases, ≤ 0.6 nm), and (2) the order of the Au NP + TiO₂ film addition to the silica supports does not affect the thickness of the latter. On the basis of the rate of pore diameter reduction measured versus the number of ALD cycles (expressed in terms of nm/cycle), the particularly narrow pore size distributions obtained after two ALD TiO₂ cycles, and previous data from our group [26,29,31], we estimate that two ALD cycles yield a TiO₂

coverage close to a monolayer. The amount of TiO_2 deposited on the SBA-15 surface, as estimated using ICP-AES measurements, was approximately 1.00 and 1.65 mmol/g catalyst after the first and second ALD cycles, respectively [31].

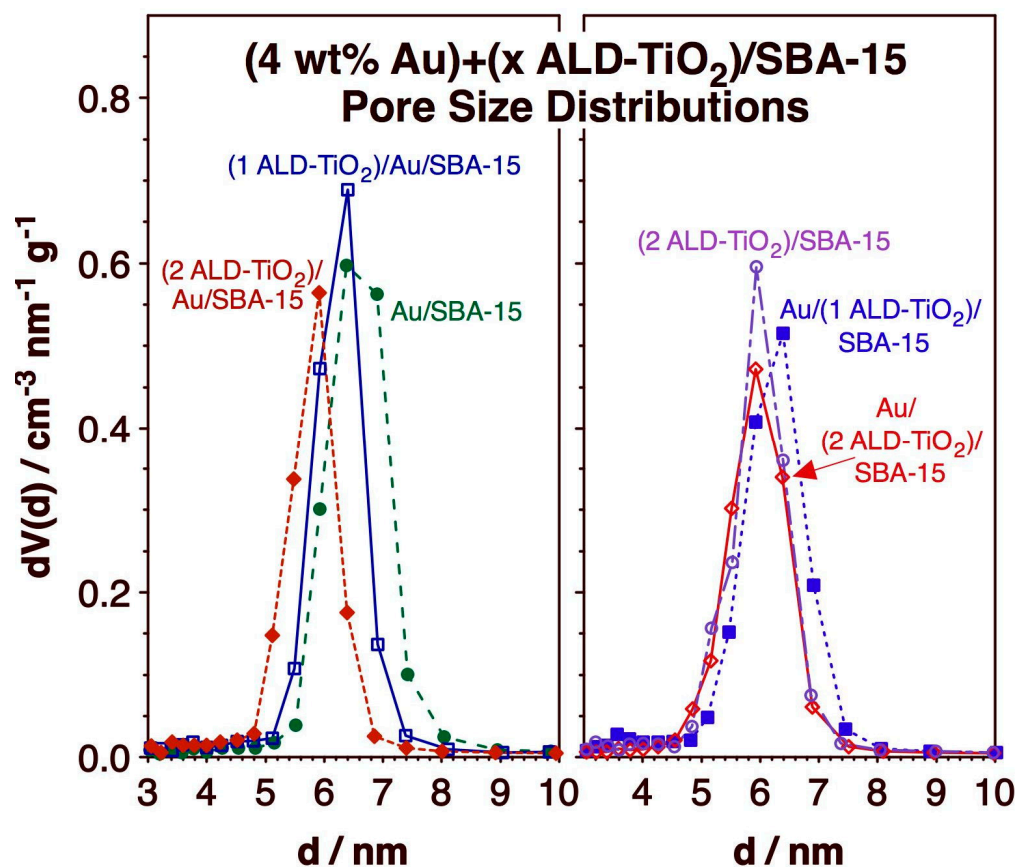


Figure 2. Pore size distributions, extracted from N_2 adsorption–desorption isotherms, for $\text{Au} + (x \text{ ALD-TiO}_2)/\text{SBA-15}$ catalysts as a function of the number of ALD cycles used (1 or 2) and of the order of the Au NP + TiO_2 film addition. Data are also provided for Au/SBA-15 and $(2 \text{ ALD-TiO}_2)/\text{SBA-15}$ samples for reference.

All of the geometrical parameters extracted from the analysis of the N_2 adsorption–desorption isotherms are reported in Figure 3. In addition to the average pore diameters discussed above, which follow identical sequences regardless of the order of the Au NP + TiO_2 film deposition (within our experimental accuracy; Figure 3, right panel), this figure shows the values calculated for the total area A (left panel) and total pore volume V (center panel). As expected, both of these parameters decrease monotonically with increasing number of TiO_2 ALD cycles, both in an approximately linear fashion. Some differences are apparent in this figure between the data for the $\text{Au}/(x \text{ ALD-TiO}_2)/\text{SBA-15}$ (where the TiO_2 film was deposited first; blue traces) and $(x \text{ ALD-TiO}_2)/\text{Au}/\text{SBA-15}$ (where TiO_2 was added after Au deposition; red traces) samples, especially after one TiO_2 ALD cycle, but the deviations are within our experimental error (see error bars in Figure 3) and are likely not significant. It is concluded that uniform thin TiO_2 films can be deposited on SBA-15 in a controlled manner via ALD and that the structural characteristics of these films are the same regardless of whether the Au NPs are deposited before or after the titania film growth. They are also similar to those already reported for TiO_2 ALD on pristine SBA-15: amorphous, and initially of quite low density, grown via the formation of individual tetrahedral Ti–oxide units on isolated Si–OH surface groups, with unusually long Ti–O bonds [26,29,31].

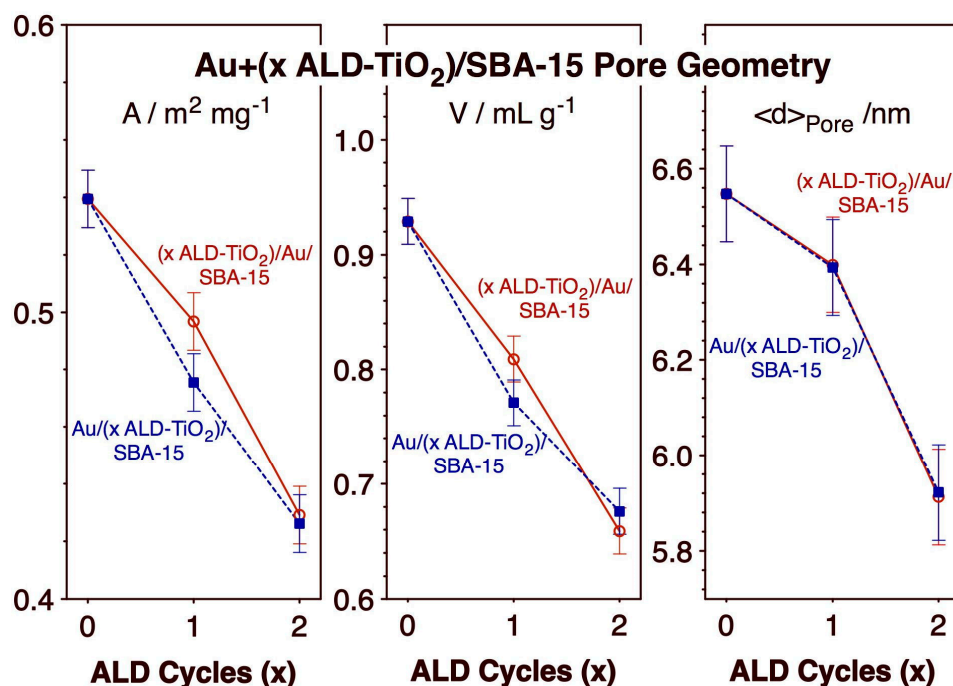


Figure 3. Titania films' geometrical parameters extracted from N₂ adsorption–desorption isotherms for Au + (x ALD-TiO₂)/SBA-15 catalysts, as a function of the number of ALD cycles used (1 or 2) and of the order of the Au NP + TiO₂ film addition. Trends are reported for the total surface area A (left panel), total pore volume V (center), and average pore diameter $\langle d \rangle_{\text{pore}}$ (right).

The nature of the Au NPs in our Au + (x ALD-TiO₂)/SBA-15 catalysts, namely, the NP size distributions and dispersion, were assessed using transmission electron microscopy (TEM). Typical TEM images and NP size distributions for the four main catalysts studied here, namely for Au/(x ALD-TiO₂)/SBA-15 and (x ALD-TiO₂)/Au/SBA-15 (x = 1 or 2), are shown in Figure 4. Three main conclusions can be extracted from these images: (1) the average Au NP diameter of all of the catalysts is slightly larger than 3 nm, and approximately the same in all samples; (2) the size distributions are reasonably narrow, with an average standard deviation of less than 1 nm; and (3) the Au NPs appear to be well dispersed within the pores of the SBA-15 support.

Au+(x ALD-TiO₂)/SBA15 TEM & NP Size Distributions

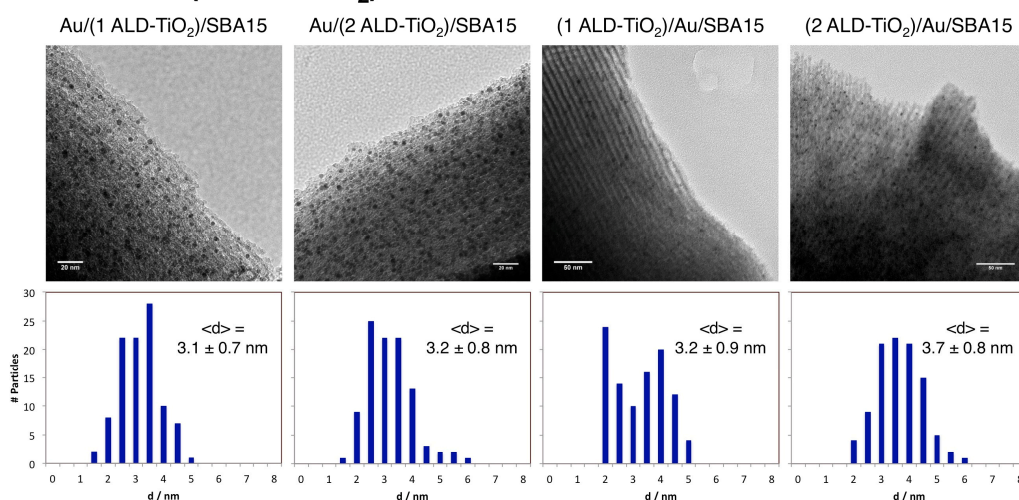


Figure 4. TEM images (top row) and Au NP size distributions (bottom row) for the Au + (x ALD-TiO₂)/SBA-15 catalysts (x = 1 or 2).

The kinetics of the oxidation of carbon monoxide with molecular oxygen promoted by our Au + (x ALD-TiO₂)/SBA-15 catalysts were tested using transmission infrared absorption spectroscopy [32]. Premixed CO + O₂ mixtures with preset molecular ratios were added to our IR cell, which acted as a batch reactor, and IR spectra were acquired versus time after heating the catalyst and cell to the desired temperature, typically 425 K. The raw IR spectra recorded for a typical case, for the conversion of 100 Torr CO plus 100 Torr O₂ at 425 K promoted by the (2 ALD-TiO₂)/Au/SBA-15 catalyst (where the Au NP deposition was followed by two ALD titania cycles), are shown in Figure 5. Even though the IR cell is designed so that the IR beam traverses through the solid catalyst, the IR absorption recorded here is dominated by the gas species; the signals from any adsorbed species are orders of magnitude weaker, and no attempt was made to extract that information. What can be seen in the IR traces in Figure 5 are two sets of doublets around 2050–2240 and 2240–2400 cm⁻¹ corresponding to gas-phase CO and gas-phase CO₂, respectively. It can be clearly observed that the CO signal decreases in intensity with increasing time, at the expense of the growth of the spectral features associated with CO₂. The respective areas of these two sets of peaks were used to quantify the conversion and to follow its kinetics.

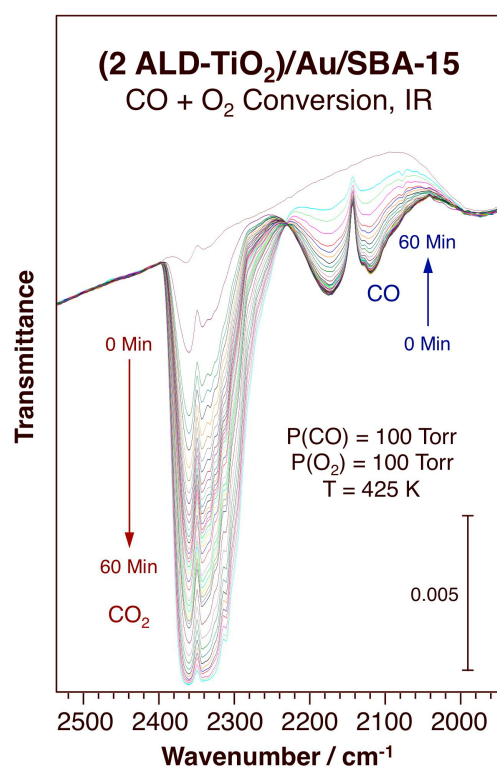


Figure 5. IR spectra versus reaction time for the conversion of 100 Torr CO + 100 Torr O₂ at 425 K, promoted by the (2 ALD-TiO₂)/Au/SBA-15 catalyst.

The results from such an analysis are illustrated in Figure 6, which displays the data for the conversion of mixtures of 50 Torr CO + 50 Torr O₂ promoted by the Au/(2 ALD-TiO₂)/SBA-15 catalyst (where two cycles of titania ALD were followed by the deposition of the Au NPs) at four different temperatures (300, 355, 425, and 525 K). The decrease in CO pressure and the accumulation of CO₂ versus reaction time inside our IR cell are graphed in the left and center panels of the figure, respectively, and the corresponding reaction rates, estimated via numerical derivation of those plots, are shown in the right panel. It should be noted that the CO and CO₂ pressures were calculated by scaling the corresponding IR peak areas (when plotted in absorbance units), assuming a linear dependence between the two parameters (Beer–Lambert law); because in reality a deviation from such linearity was found in blank studies of IR signal intensity versus CO pressure,

especially in the high-pressure limit (possibly because of signal saturation in the IR detector), a measurable systematic deviation from the true pressure values was introduced by our analysis, with the CO₂ production rates consistently appearing to be larger than those of the CO consumption [33]. Average rates are used in some of our subsequent discussions to account for this discrepancy, and the differences between the CO and CO₂ measurements were employed to estimate the experimental error bars.

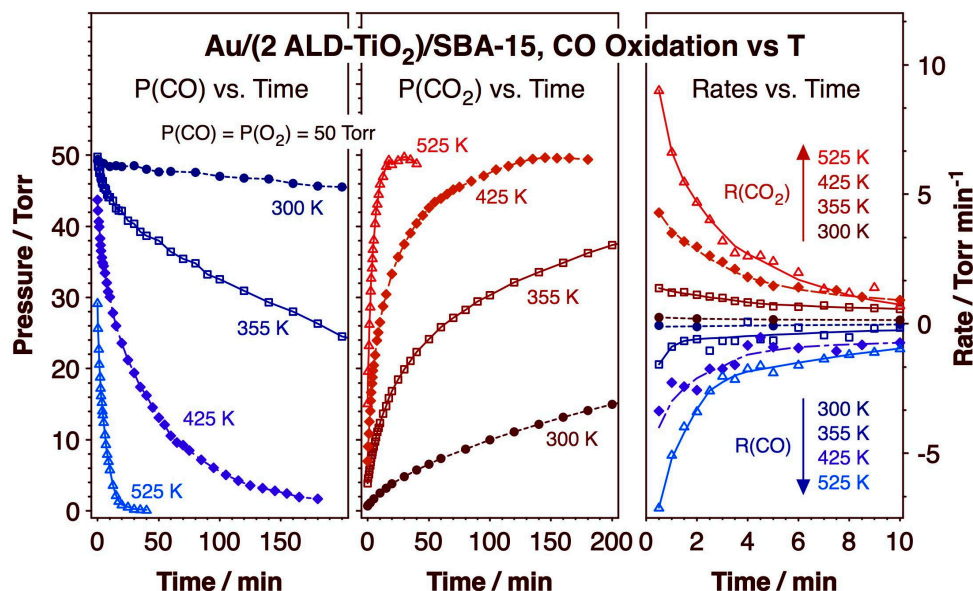


Figure 6. Kinetics of CO oxidation promoted by the Au/(2 ALD-TiO₂)/SBA-15 catalyst as a function of temperature. **Left:** CO pressure versus time. **Center:** CO₂ pressure versus time. **Right:** rates of change in CO (blue symbols: negative values) and CO₂ (red symbols: positive values) pressures versus time. Initial CO and O₂ pressures: 50 Torr each.

Figure 7 displays an Arrhenius plot of the initial reaction rates for the CO oxidation reaction promoted by our Au/(2 ALD-TiO₂)/SBA-15 catalyst, estimated from the data in Figure 6. Both rates for CO consumption (blue filled squares) and CO₂ production (red filled circles) are reported. An apparent activation barrier of $E_a = 22.6 \pm 0.9$ kJ/mol was estimated from this graph. This value is relatively low when compared to those of other oxidation reactions, but in the range of what has been reported for CO oxidations promoted by Au-based catalysts [16,34,35]. For reference, CO conversion with an equivalent Au/SBA-15 catalyst, without any titania films, was determined to take place at rates below half of those reported here with the Au + (x ALD-TiO₂)/SBA-15 catalysts. ALD-TiO₂/SBA-15 exhibited no measurable catalytic activity.

The dependence of the CO oxidation rate on CO and O₂ gas partial pressures and on the nature of the catalysts was probed next. Figure 8 displays the raw kinetic data in terms of the evolution of the CO (left panel) and CO₂ (right) partial pressures versus reaction time, whereas Figure 9 reports the data in the form of the logarithm of the reaction rates (CO₂ production) versus the logarithm of the CO partial pressure as the reactions proceed. In both cases, five sets of data are reported, for the 50 Torr CO + 50 Torr O₂ (dark blue filled circles), 50 Torr CO + 150 Torr O₂ (purple filled diamonds), and 100 Torr CO + 100 Torr O₂ (dark red filled squares) initial mixtures with the Au/(2 ALD-TiO₂)/SBA-15 catalyst, as well as for the 50 Torr CO + 50 Torr O₂ (light blue open circles) and 100 Torr CO + 100 Torr O₂ (light red open squares) initial mixtures with the (2 ALD-TiO₂)/Au/SBA-15 catalyst. We first focus on the differences in catalytic activities seen between the two catalysts. It is clear in the two examples where the same set of initial pressures were used with both catalysts, namely, for the 50 Torr:50 Torr and 100 Torr:100 Torr CO:O₂ ratios, that the conversion with the (2 ALD-TiO₂)/Au/SBA-15 catalyst is slower than that with the Au/(2 ALD-TiO₂)/SBA-15 sample. To explain this difference, it is useful to remember that both the TiO₂ film

thicknesses (Figures 2 and 3) and the Au NP size distributions (Figure 4) are similar in both catalysts; these properties cannot account for the different catalytic activity reported here. It is possible that in the case where the Au NPs are deposited first, the subsequent TiO₂ ALD growth may lead to the partial covering of the metal surface. Alternatively, depositing the Au NPs on the TiO₂ film may lead to a larger metal–oxide perimeter and thus to the formation of more interfacial sites than if the titania film is added afterward. Future work will be needed to address this issue.

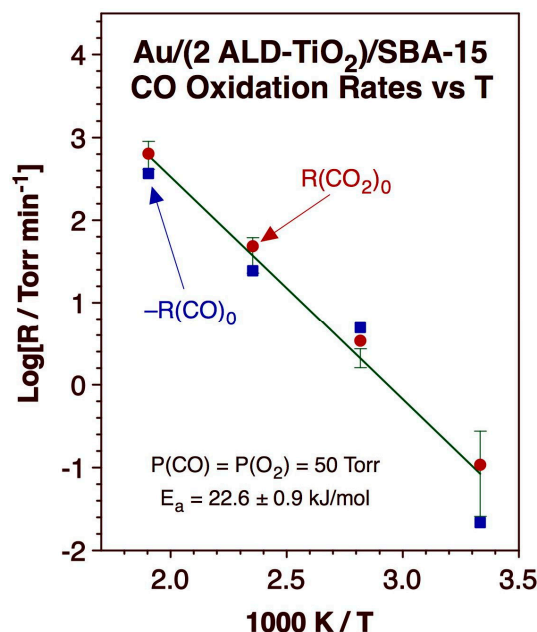


Figure 7. Arrhenius plot of the initial reaction rates for CO oxidation promoted by our Au/(2 ALD-TiO₂)/SBA-15 catalyst. Initial CO and O₂ pressures: 50 Torr each. The red filled circles and blue filled squares correspond to the experimental data for the rates of CO₂ production and CO consumption, respectively, whereas the green line is the result of a least square fit to all of the data.

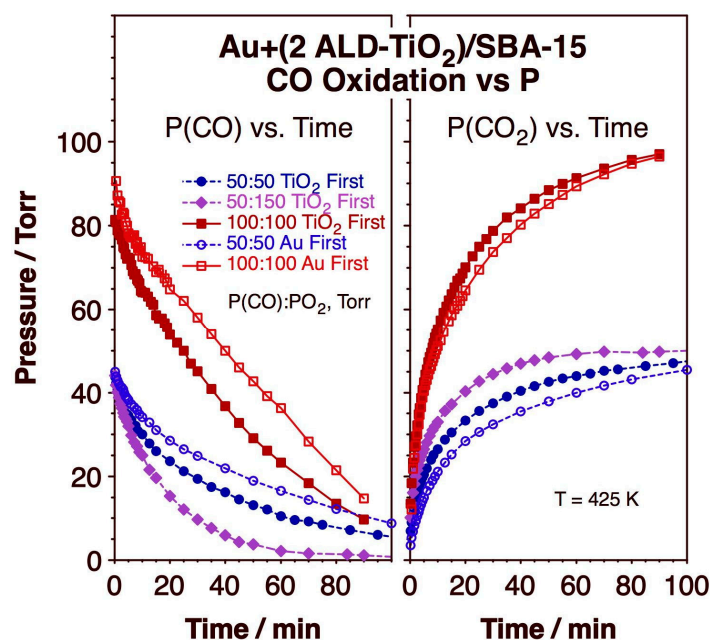


Figure 8. Kinetics of CO oxidation with O₂ promoted by the (2 ALD-TiO₂)/Au/SBA-15 and Au/(2 ALD-TiO₂)/SBA-15 catalysts as a function of the initial CO and O₂ partial pressures. The evolution of the CO (left panel) and CO₂ (right) partial pressures versus reaction time is shown.

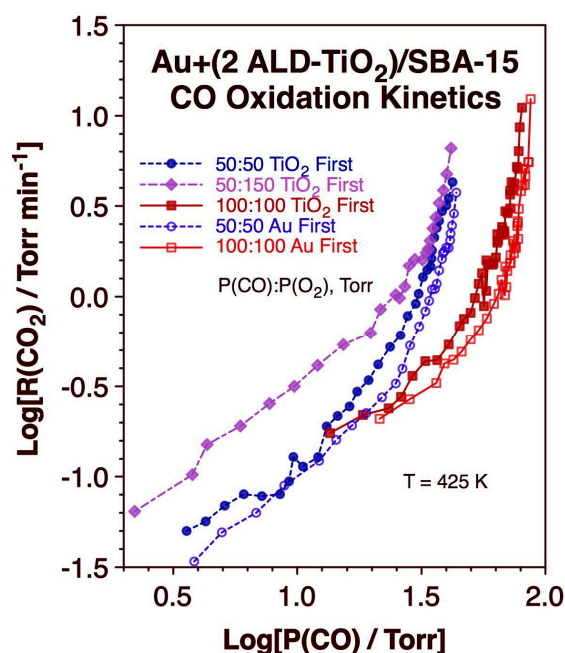


Figure 9. The same kinetics of the CO oxidation reaction promoted by the (2 ALD-TiO₂)/Au/SBA-15 and Au/(2 ALD-TiO₂)/SBA-15 catalysts as a function of the initial CO and O₂ partial pressures shown in Figure 8, but here displayed as the dependence of the logarithm of the CO₂ production rate on the logarithm of the CO partial pressure.

It can also be seen from the data in Figures 8 and 9 that the kinetics of the CO oxidation are complex, since the dependence of the reaction rate on the CO and O₂ partial pressures does not follow a simple rate law. Indeed, Figure 9 highlights how the total reaction order, extracted from the slope of plots of $\log[R(\text{CO}_2)]$ versus $\log[P(\text{CO})]$, displays two regimes, transitioning from a high value of approximately 4 at the start of the reaction to a number closer to 1 toward the end of the conversion, as the CO is depleted. These data also clearly show that the initial rates are highly sensitive to $P(\text{CO})$ but not so much to $P(\text{O}_2)$. For instance, with the Au/(2 ALD-TiO₂)/SBA-15 catalyst, the initial rate only changes from 4.3 Torr/min to 6.6 Torr/min (a ~50% increase) as the initial O₂ pressure is tripled from 50 to 150 Torr (keeping the initial CO pressure the same, at 50 Torr), but it reaches a value of 11 Torr/min with the 100 Torr:100 Torr CO:O₂ mixture. This is consistent with reaction rate orders of about 1 and ≤ 0.5 with respect to CO and O₂, respectively, and suggests a rate-limiting step involving the recombination of one CO molecule and one oxygen atom on the surface of the catalyst (on Au sites, most likely [36,37]). On the other hand, $P(\text{O}_2)$ seems to become more important in determining the reaction rate at later stages of the conversion, as the traces for the 50 Torr:50 Torr and 50 Torr:150 Torr CO:O₂ ratios diverge from each other (with the Au/(2 ALD-TiO₂)/SBA-15 catalyst; Figure 9); the values in the latter case become approximately three times as large of those in the former, consistent with a first order dependence on $P(\text{O}_2)$. Concurrently, the effect of $P(\text{CO})$ becomes less noticeable, and the order of the reaction rate with respect to CO appears to become negative, to the point where the rates with the 100 Torr:100 Torr CO:O₂ mixtures eventually become smaller than with the 50 Torr:50 Torr CO:O₂ combination (with both catalysts). At this point, it can be said that the uptake of O₂ on the catalytic surface sites may be the rate-limiting step, and that O₂ may compete with CO for adsorption sites.

3. Discussion

The focus of this work has been to control the creation of metal–oxide interface sites in Au-TiO₂ catalysts using ALD to tune the thickness of the titania films on a sub-monolayer scale, and to possibly modify the nature of these sites by alternating the order in which the Au NPs and the TiO₂ films are added to the support (SBA-15, a well-defined mesoporous

silica material). N_2 adsorption–desorption isothermal measurements indicated that neither the thickness nor the uniformity of the titania films are affected by the presence of the Au NPs on the surface (Figures 2 and 3), and electron microscopy imaging provided evidence for the similarity of the Au NP size average and distribution when deposited on the silica versus titania surfaces (Figure 4). All of this suggests that the deposition order during the synthesis of the Au + (x ALD-TiO₂)/SBA-15 catalysts should not make a difference in terms of the nature of the resulting catalysts. On the other hand, kinetic data on the oxidation of carbon monoxide with molecular oxygen clearly indicate that this is not the case.

Indeed, it was determined that CO oxidation is slower on the samples where Au is deposited first (Figures 8 and 9). In addition, the mechanism of the reaction appears to evolve and change as the CO conversion to CO₂ proceeds. Initially, a high total order for the reaction rate was estimated to reflect a rate-limiting step where adsorbed CO recombines with surface atomic oxygen, likely at Au sites [36,37]. As the reaction proceeds, however, the kinetic behavior is altered and the total reaction order is reduced; the new rate-limiting step becomes the uptake of molecular O₂, quite possibly at the Au-TiO₂ interface sites. The analysis of the kinetic data acquired as a function of the CO + O₂ gas mixture composition suggests that the number of the catalytic sites that activate the O=O bond, at the Au-TiO₂ interface, decreases as the reaction proceeds, and that such a step becomes slower than the recombination of CO + O on the Au surface that controls the rate in the initial stages of the process. It would appear that, in order to maximize the performance of the catalyst in terms of long-term stability, it is desirable to increase and sustain the surface coverage of Au-TiO₂ interface sites. By facilitating the activation of O₂ and inducing a switch to a CO oxidation process where the recombination of CO + O adsorbed species is rate-limiting, at least in the initial stages of the reaction, ALD was shown here to be a promising approach to accomplish this goal. However, more work is still needed to optimize the synthesis and improve the stability of the resulting catalysts over the course of oxidation reactions.

What is clear at this stage is that ALD affords the addition of TiO₂ to catalyst supports in a controlled manner, with sub-monolayer thickness control either before or after metal deposition. The addition of thin films of active oxides such as titania to inert supports in catalyst preparation, rather than using bulk materials of that active oxide directly, introduces the capability of creating new surface sites, both in metal–oxide interfaces and within mixed-oxide thin surface films. It also helps with spectroscopic discrimination between surface and bulk phases (via XPS, for instance), potentially facilitating the detection of minority surface sites such as oxygen vacancies (i.e., Ti³⁺ sites) or metal–oxide synergistic ensembles (i.e., Au⁺–O–Ti⁴⁺). This flexibility can be extended to other systems and catalytic problems, and therefore ALD can be viewed as a fairly general synthetic method.

4. Materials and Methods

The catalysts used in this study were prepared via the deposition of both Au NPs and TiO₂ thin films on a commercial SBA-15 silica mesoporous support (Sigma-Aldrich, research purity). For the Au NP deposition, a variation of a reported procedure [38] was followed, where 17.2 mg of Au(en)₂Cl₃ was first added to 15 mL H₂O to produce a light-yellow solution with a pH of approximately 4.5. A 0.2 M NaOH solution was added dropwise to tune the pH to 10, at which point the color of the solution changed to a more intense yellow. 200 mg SBA-15 was then added, at which point the pH dropped to 6.5; again, 0.2 M NaOH was used to adjust the pH back to 10. The solution was stirred for 2 h, and the solid was filtered and washed with H₂O. The resulting light-yellow powder was kept in a desiccator for at least 24 h under a vacuum. The catalyst was calcined at 675 K for 2 h and reduced at 525 K under a H₂ atmosphere for 3 h prior to its use [39]. The theoretical metal (Au) loading of all samples was 4 wt%.

The TiO₂ ALD was carried out in a homemade batch reactor described in more detail elsewhere [26,28,29,31] by alternating exposures to tetrakis(dimethylamido)Ti(IV) (TDMAT, Aldrich-Sigma, 99.999% purity on a trace metal basis; heated to 315 K during the ALD processes) and deionized water at 375 K. Typical cycle times were TDMAT:N₂:H₂O:N₂ =

20 min:50 min:10 min:50 min. In the samples studied here, either 1 or 2 ALD cycles were carried out, either before or after Au NP deposition. The resulting samples are labeled in the text and figures as (x ALD-TiO₂)/Au/SBA-15 or Au/(x ALD-TiO₂)/SBA-15, depending on whether the Au was deposited before or after the titania, respectively (Au + (x ALD-TiO₂)/SBA-15 is used generically to refer to both options together); x = 1 or 2 stands for the number of TiO₂ ALD cycles used.

The scanning transmission electron microscopy (STEM) images were acquired using a Philips Tecnai 12 instrument (120 kV accelerating voltage). N₂ adsorption–desorption isotherms were acquired using a NOVA@2000e gas sorption system, and the resulting data were analyzed using Nova Win software; pore diameter distributions and total pore volumes were estimated from the data for the desorption branch using the BJH (Barrett–Joyner–Halenda) equations [40] for type IV isotherms [41], whereas total surface areas were calculated using the BET (Brunauer–Emmett–Teller) isotherm formula [42]. The TiO₂ and Au loadings were measured using PerkinElmer Optima 7300DV inductively coupled plasma atomic emission spectroscopy (ICP-AES) apparatus [31].

The in situ transmission infrared spectroscopy (IR) kinetic experiments were performed using a Bruker Tensor 27 Fourier transform infrared (FTIR) spectrometer equipped with a deuterated triglycine sulfate (DTGS) detector. About 10 mg of the catalyst was pressed into a self-supporting wafer and loaded inside a homemade quartz cell with NaCl windows [43]. The pellet was degassed in the cell at 425 K for 2 h under vacuum, after which the cell was heated to 625 K and filled with 200 mTorr O₂. The oxidation pretreatment was carried out for 1 h, followed by pumping and cell refilling with 200 mTorr H₂ for 1 h to reduce the catalyst; the H₂ was then pumped out. This O₂/H₂ pretreatment cycle was repeated two more times. Before the CO oxidation experiments, a background IR scan was carried out while evacuating the cell using a mechanical pump. For the kinetic experiments, the cell was then filled with premixed CO + O₂ gas mixtures (with preset CO:O₂ molar ratios) to the pressures indicated in the corresponding figures, the temperature was increased to the desired value, and IR spectra were taken periodically as the oxidation reaction proceeded.

5. Conclusions

A new approach was tested for the preparation of Au-TiO₂-based catalysts where the thickness of the oxide film was tuned using ALD and the amount and nature of metal–oxide interface sites were controlled by setting a specific deposition order. It was shown that the ALD of titania films can be used to deposit as little as half a monolayer of TiO₂ in a uniform and reproducible fashion on silica supports, and that the order of this deposition, before versus after the growth of Au NPs, does not affect the geometrical characteristics of either the metal or the oxide phases. The resulting catalysts were shown to promote the oxidation of CO. The apparent activation barrier for this reaction was estimated to be $E_a = 22.6 \pm 0.9$ kJ/mol, a value comparable to that obtained with other Au/TiO₂ catalysts where the titanium oxide is in bulk rather than thin film form. The kinetics of the reaction were shown to be complex, with a total order of the reaction rate that changes as the reaction proceeds. The data were interpreted as the result of a change in the rate-limiting step within the reaction mechanism, from an initial CO + O recombination step on the Au surface at the start to the activation of O₂ on metal–oxide interface sites at later times. We speculate that optimizing the number of available interface sites needed to promote O₂ dissociation may be well achieved using ALD as a way to add the titania (or another reducible oxide) phase to these catalysts.

Author Contributions: X.Q.: supervision and performance of most experiments, initial data analysis; W.K.: help with the synthesis and catalytic testing of the catalysts and with data analysis; Y.V.: growth and characterization of the titania films via ALD; I.L.: electron microscopy analysis of the Au-containing catalysts; F.Z.: conception and supervision of the project; final data analysis, writing of the manuscript. All authors have read and agreed to the published version of the manuscript.

Funding: Financial support for this project was provided by a grant from the U.S. Department of Energy, Office of Science, Basic Energy Sciences, Chemical Transformations Division, Catalysis Science Program, under award no. DE-SC0023119.

Data Availability Statement: The data presented in this study are available upon request from the corresponding author.

Conflicts of Interest: The authors declare no conflict of interest.

References

1. Cavani, F. Catalytic selective oxidation: The forefront in the challenge for a more sustainable chemical industry. *Catal. Today* **2010**, *157*, 8–15. [[CrossRef](#)]
2. Guo, Z.; Liu, B.; Zhang, Q.; Deng, W.; Wang, Y.; Yang, Y. Recent advances in heterogeneous selective oxidation catalysis for sustainable chemistry. *Chem. Soc. Rev.* **2014**, *43*, 3480–3524. [[CrossRef](#)] [[PubMed](#)]
3. Hagen, J. *Industrial Catalysis: A Practical Approach*, 3rd ed.; Wiley: Weinheim, Germany, 2015; p. 544.
4. Védrine, J.C.; Fechete, I. Heterogeneous partial oxidation catalysis on metal oxides. *Comptes Rendus Chim.* **2016**, *19*, 1203–1225. [[CrossRef](#)]
5. Hutchings, G.J.; Haruta, M. A golden age of catalysis: A perspective. *Appl. Catal. A* **2005**, *291*, 2–5. [[CrossRef](#)]
6. Bond, G.C.; Louis, C.; Thompson, D.T. *Catalysis by Gold*; Imperial College Press; World Scientific Publishing: London, UK, 2006; p. 384.
7. Min, B.K.; Friend, C.M. Heterogeneous gold-based catalysis for green chemistry: Low-temperature CO oxidation and propene oxidation. *Chem. Rev.* **2007**, *107*, 2709–2724. [[CrossRef](#)]
8. Lee, I.; Joo, J.B.; Yin, Y.; Zaera, F. A Yolk@Shell Nanoarchitecture for Au/TiO₂ Catalysts. *Angew. Chem. Int. Ed.* **2011**, *50*, 10208–10211. [[CrossRef](#)]
9. Panayotov, D.A.; Morris, J.R. Surface chemistry of Au/TiO₂: Thermally and photolytically activated reactions. *Surf. Sci. Rep.* **2016**, *71*, 77–271. [[CrossRef](#)]
10. Zaera, F. Gold-Titania Catalysts for Low-Temperature Oxidation and Water Splitting. *Top. Catal.* **2018**, *61*, 336–347. [[CrossRef](#)]
11. Lee, I.; Zaera, F. Catalytic oxidation of carbon monoxide at cryogenic temperatures. *J. Catal.* **2014**, *319*, 155–162. [[CrossRef](#)]
12. Lee, I.; Joo, J.B.; Yin, Y.; Zaera, F. Au@Void@TiO₂ yolk-shell nanostructures as catalysts for the promotion of oxidation reactions at cryogenic temperatures. *Surf. Sci.* **2016**, *648*, 150–155. [[CrossRef](#)]
13. Lee, I.; Zaera, F. Effect of metal nanoparticle size and titania crystallinity on the performance of Au/TiO₂ catalysts for the promotion of carbon monoxide oxidation at cryogenic temperatures. *J. Chem. Phys.* **2019**, *151*, 054701. [[CrossRef](#)]
14. Lee, I.; Zaera, F. Use of Au@Void@TiO₂ yolk-shell nanostructures to probe the influence of oxide crystallinity on catalytic activity for low-temperature oxidations. *J. Chem. Phys.* **2019**, *151*, 234706. [[CrossRef](#)] [[PubMed](#)]
15. Ishida, T.; Murayama, T.; Taketoshi, A.; Haruta, M. Importance of Size and Contact Structure of Gold Nanoparticles for the Genesis of Unique Catalytic Processes. *Chem. Rev.* **2020**, *120*, 464–525. [[CrossRef](#)] [[PubMed](#)]
16. Green, I.X.; Tang, W.; Neurock, M.; Yates, J.T., Jr. Spectroscopic observation of dual catalytic sites during oxidation of CO on a Au/TiO₂ catalyst. *Science* **2011**, *333*, 736–739. [[CrossRef](#)]
17. Liu, X.Y.; Wang, A.; Zhang, T.; Mou, C.-Y. Catalysis by gold: New insights into the support effect. *Nano Today* **2013**, *8*, 403–416. [[CrossRef](#)]
18. Yu, L.; Liu, Y.; Yang, F.; Evans, J.; Rodriguez, J.A.; Liu, P. CO Oxidation on Gold-Supported Iron Oxides: New Insights into Strong Oxide–Metal Interactions. *J. Phys. Chem. C* **2015**, *119*, 16614–16622. [[CrossRef](#)]
19. Odarchenko, Y.; Martin, D.J.; Arnold, T.; Beale, A.M. CO oxidation over supported gold nanoparticles as revealed by operando grazing incidence X-ray scattering analysis. *Faraday Discuss.* **2018**, *208*, 243–254. [[CrossRef](#)] [[PubMed](#)]
20. Ferraz, C.P.; Navarro-Jaén, S.; Rossi, L.M.; Dumeignil, F.; Ghazzal, M.N.; Wojcieszak, R. Enhancing the activity of gold supported catalysts by oxide coating: Towards efficient oxidations. *Green Chem.* **2021**, *23*, 8453–8457. [[CrossRef](#)]
21. O'Neill, B.J.; Jackson, D.H.K.; Lee, J.; Canlas, C.; Stair, P.C.; Marshall, C.L.; Elam, J.W.; Kuech, T.F.; Dumesic, J.A.; Huber, G.W. Catalyst Design with Atomic Layer Deposition. *ACS Catal.* **2015**, *5*, 1804–1825. [[CrossRef](#)]
22. Singh, J.A.; Yang, N.; Bent, S.F. Nanoengineering Heterogeneous Catalysts by Atomic Layer Deposition. *Annu. Rev. Chem. Biomol. Eng.* **2017**, *8*, 41–62. [[CrossRef](#)]
23. Onn, T.M.; Küngas, R.; Fornasiero, P.; Huang, K.; Gorte, R.J. Atomic Layer Deposition on Porous Materials: Problems with Conventional Approaches to Catalyst and Fuel Cell Electrode Preparation. *Inorganics* **2018**, *6*, 34. [[CrossRef](#)]
24. Zaera, F. Molecular approaches to heterogeneous catalysis. *Coord. Chem. Rev.* **2021**, *448*, 214179. [[CrossRef](#)]
25. Zaera, F. Designing Sites in Heterogeneous Catalysis: Are We Reaching Selectivities Competitive with Those of Homogeneous Catalysts? *Chem. Rev.* **2022**, *122*, 8594–8757. [[CrossRef](#)] [[PubMed](#)]
26. Weng, Z.; Chen, Z.-h.; Qin, X.; Zaera, F. Sub-monolayer control of the growth of oxide films on mesoporous materials. *J. Mater. Chem. A* **2018**, *6*, 17548–17558. [[CrossRef](#)]
27. Weng, Z.; Zaera, F. Sub-Monolayer Control of Mixed-Oxide Support Composition in Catalysts via Atomic Layer Deposition: Selective Hydrogenation of Cinnamaldehyde Promoted by (SiO₂-ALD)-Pt/Al₂O₃. *ACS Catal.* **2018**, *8*, 8513–8524. [[CrossRef](#)]

28. Weng, Z.; Zaera, F. Atomic Layer Deposition (ALD) as a Way to Prepare New Mixed-Oxide Catalyst Supports: The Case of Alumina Addition to Silica-Supported Platinum for the Selective Hydrogenation of Cinnamaldehyde. *Top. Catal.* **2019**, *62*, 838–848. [[CrossRef](#)]
29. Ke, W.; Qin, X.; Palomino, R.M.; Simonovis, J.P.; Senanayake, S.D.; Rodriguez, J.A.; Zaera, F. Redox Properties of TiO₂ Thin Films Grown on Mesoporous Silica by Atomic Layer Deposition. *J. Phys. Chem. Lett.* **2023**, *14*, 4696–4703. [[CrossRef](#)]
30. Rasteiro, L.F.; Motin, M.A.; Vieira, L.H.; Assaf, E.M.; Zaera, F. Growth of ZrO₂ films on mesoporous silica sieve via atomic layer deposition. *Thin Solid Films* **2023**, *768*, 139716. [[CrossRef](#)]
31. Ke, W.; Liu, Y.; Wang, X.; Qin, X.; Chen, L.; Palomino, R.M.; Simonovis, J.P.; Lee, I.; Waluyo, I.; Rodriguez, J.A.; et al. Nucleation and Initial Stages of Growth during the Atomic Layer Deposition of Titanium Oxide on Mesoporous Silica. *Nano Lett.* **2020**, *20*, 6884–6890. [[CrossRef](#)]
32. Zaera, F. Infrared Absorption Spectroscopy of Adsorbed CO: New Applications in Nanocatalysis for an Old Approach. *Chem-CatChem* **2012**, *4*, 1525–1533. [[CrossRef](#)]
33. Zaera, F. New advances in the use of infrared absorption spectroscopy for the characterization of heterogeneous catalytic reactions. *Chem. Soc. Rev.* **2014**, *43*, 7624–7663. [[CrossRef](#)] [[PubMed](#)]
34. Bond, G.; Thompson, D. Gold-catalysed oxidation of carbon monoxide. *Gold Bull.* **2000**, *33*, 41–50. [[CrossRef](#)]
35. Schubert, M.M.; Hackenberg, S.; van Veen, A.C.; Muhler, M.; Plzak, V.; Behm, R.J. CO Oxidation over Supported Gold Catalysts—“Inert” and “Active” Support Materials and Their Role for the Oxygen Supply during Reaction. *J. Catal.* **2001**, *197*, 113–122. [[CrossRef](#)]
36. Chen, M.; Goodman, D.W. Catalytically active gold on ordered titania supports. *Chem. Soc. Rev.* **2008**, *37*, 1860–1870. [[CrossRef](#)] [[PubMed](#)]
37. Herzing, A.A.; Kiely, C.J.; Carley, A.F.; Landon, P.; Hutchings, G.J. Identification of Active Gold Nanoclusters on Iron Oxide Supports for CO Oxidation. *Science* **2008**, *321*, 1331–1335. [[CrossRef](#)] [[PubMed](#)]
38. Tsai, C.-H.; Xu, M.; Kunal, P.; Trewyn, B.G. Aerobic oxidative esterification of primary alcohols over Pd-Au bimetallic catalysts supported on mesoporous silica nanoparticles. *Catal. Today* **2018**, *306*, 81–88. [[CrossRef](#)]
39. Zhu, H.; Liang, C.; Yan, W.; Overbury, S.H.; Dai, S. Preparation of Highly Active Silica-Supported Au Catalysts for CO Oxidation by a Solution-Based Technique. *J. Phys. Chem. B* **2006**, *110*, 10842–10848. [[CrossRef](#)]
40. Barrett, E.P.; Joyner, L.G.; Halenda, P.P. The Determination of Pore Volume and Area Distributions in Porous Substances. I. Computations from Nitrogen Isotherms. *J. Am. Chem. Soc.* **1951**, *73*, 373–380. [[CrossRef](#)]
41. Sing, K.S.W.; Everett, D.H.; Haul, R.A.W.; Moscou, L.; Pierotti, R.A.; Rouquerol, J.; Siemieniewska, T. Reporting Physisorption Data for Gas/Solid Systems with Special Reference to the Determination of Surface Area and Porosity. *Pure Appl. Chem.* **1985**, *57*, 603–619. [[CrossRef](#)]
42. Brunauer, S.; Emmett, P.H.; Teller, E. Adsorption of Gases in Multimolecular Layers. *J. Am. Chem. Soc.* **1938**, *60*, 309–319. [[CrossRef](#)]
43. Cao, Y.; Chen, B.; Guerrero-Sánchez, J.; Lee, I.; Zhou, X.; Takeuchi, N.; Zaera, F. Controlling Selectivity in Unsaturated Aldehyde Hydrogenation Using Single-Site Alloy Catalysts. *ACS Catal.* **2019**, *9*, 9150–9157. [[CrossRef](#)]

Disclaimer/Publisher’s Note: The statements, opinions and data contained in all publications are solely those of the individual author(s) and contributor(s) and not of MDPI and/or the editor(s). MDPI and/or the editor(s) disclaim responsibility for any injury to people or property resulting from any ideas, methods, instructions or products referred to in the content.